A Small Low Angular Momentum Inertial Gyroscope

M. S. SAPUPPO* AND P. J. PIJOAN†
Charles Stark Draper Laboratory, Massachusetts Institute of Technology, Cambridge, Mass.

A single-degree-of-freedom gyroscope, less than $1\frac{1}{2}$ in. in diameter, less than 2 in. long, and weighing less than $\frac{1}{2}$ lb, has been developed for inertial guidance applications. Small size, high reliability, low power consumption, and ability to withstand extreme environments are achieved through use of a low angular momentum (2–8 × 10^3 dyne-cm-sec) wheel. A discussion of advanced material technology, subassembly design, and a computer-executed analytical model of the wheel and hence instrument performance are discussed. These are presented in terms of how they relate to the magnitude and stability of the gyroscope coefficients.

Nomenclature

D = total drift rate about output axis
D_F = gyro drift rate that is insensitive to acceleration
D_U = gyro drift rate proportional to linear acceleration
D_K = gyro drift rate proportional to linear acceleration squared
D_R = random gyro uncertainty drift rate
a_I, a_S, a_O = linear acceleration along input, spin, and output axes, respectively
D_I, D_S, D_O = drift coefficient due to linear accelerations along input, spin, and output axes, respectively
$D_{II}, D_{SS}, D_{IO}, D_{IS}, D_{OS}, D_{OO}$ = drift coefficients due to square and product of linear accelerations along input, spin, and output axes, respectively
$\omega_O, \omega_I, \omega_S$ = case angular rates with respect to inertial space about output, input, and spin axes, respectively
$\dot{\omega}_O, \dot{\omega}_I, \dot{\omega}_S$ = case angular accelerations with respect to inertial space
$I_{OO}, I_{II}, I_{SS}, I_{OS}, I_{OI}, I_{SI}$ = float moments and products of inertia
H = gyro wheel angular momentum (expressed in thousands of dyne-cm-sec)
M = total drift torque about output axis
MMF = magnetomotive force
P = permeance
θ = angle about OA
I_{ms} = magnetic suspension current
N = number of suspension turns
V_{ms} = suspension excitation voltage
Z_{ms} = suspension impedance
T_n = compensation winding torque
I_c = compensation winding current
ϕ = phase angle between I_{ms} and I_c
R_x, Z_c = compensation resistance and impedance, respectively
U_S = unblance along spin axis
U_I = unbalance along input axis
g_I = component of gravity along input axis
g_S = component of gravity along spin axis
$d\rho_f/dT$ = flotation fluid density temperature coefficient
V = float volume
T = temperature of flotation fluid
U_O = apparent unbalance along output axis
g_O = component of gravity along output axis
K_{AB} = deflection along A axis due to a unit load along B axis
m = effective mass displaced (may be different for each term)
d = deflection along input axis
K_A = axial stiffness of bearing pair
K_R = radial stiffness of bearing pair
a_O = acceleration along output axis
M_W = mass of wheel
A_a = attitude angle
R = running torque in dyne-cm

Presented as Paper 70-1011 at the AIAA Guidance, Control and Flight Mechanics Conference, Santa Barbara, Calif., August 17–19, 1970; submitted August 31, 1970; revision received April 20, 1971. The authors wish to acknowledge the contributions of the following Draper Laboratory personnel: R. Dauwalter, G. Garcia, A. Lattanzi, J. Meehan, J. Nelson, V. Readdy, J. Scoppetuolo, P. Steranka, and H. Watson.

Index category: Spacecraft Navigation, Guidance, and Flight-Path Control Systems.

* Associate Director. Member AIAA.
† Assistant Director. Member AIAA.

Introduction

THE concept of the low angular momentum gyro was derived through experience in the design and development of high-performance Pendulous Integrating Gyroscopic Accelerometers (PIGA). By utilizing the basic design principles of the gyroscopic element of the PIGA, an inertial gyroscope was obtained which has the ability to withstand high linear acceleration and high slew rates about the input axis.

This paper describes the small low angular momentum (SLAM) gyroscope. It is less than $1\frac{1}{2}$ in. in diam by 2 in. in length and weighs less than $\frac{1}{2}$ lb. Basically, the SLAM gyro consists of three separate cylindrical structures (Fig. 1). The innermost structure is the spinning wheel (angular momentum generator), which is supported by the middle structure (the float). In turn, the float is supported by the outer structure (main housing and two end housings) by means of electromagnetic suspension and flotation in a damping fluid. With this single-degree-of-freedom construction,

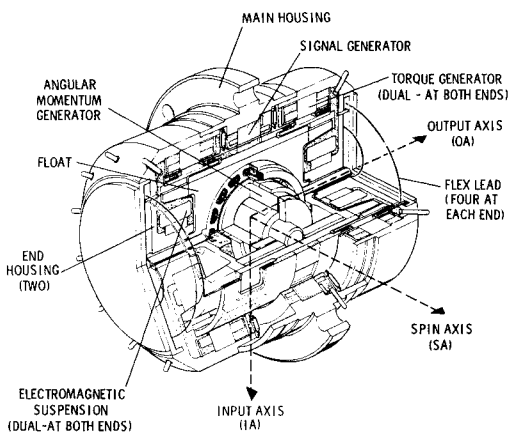

Fig. 1 SLAM gyro, cutaway view.

the gyro wheel is free to precess only in response to components of angular velocity received along the gyro input axis.

The SLAM gyro has an angular momentum of 8×10^3 dyne-cm-sec as compared to those gyros with comparable performance but having a higher angular momentum from 30 to 250×10^3 dyne-cm-sec. In general, the lower the wheel angular momentum, the smaller the size. Also, the lower the wheel angular momentum, the lower the power to drive the wheel, and for a given input rate, the lower the torque motor power required when the unit operates in the torque-to-balance mode. Thus, advantages of small size and low power both result in this gyro design.

Generally, high performance has not been associated with low angular momentum. For a given input rate, the lower the angular momentum, the lower the precessional torque about the output axis, and the higher the ratio of uncertainty torques about the output axis to the precessional torque or information containing torque. Therefore, to achieve high performance with low angular momentum requires low uncertainty torques about the output axis of the unit. The manner by which the SLAM gyro achieves this requisite is the major area of discussion in this paper. The design of the SLAM gyro entails a tradeoff between angular momentum and power to achieve small size and weight, without sacrificing performance.

SLAM Gyro Technology

Characteristics of Drift Performance

The technology of the SLAM gyro is a combination of material, fluid, electromagnetic, and hydrodynamic gas bearing developments. How the technology in these fields relate to gyro performance can, for the most part, be shown by relating them to the equations for the torque about the output axis of the single-degree-of-freedom floated integrating gyro operating in the closed servo loop, inertially stabilized mode.[1] To simplify the analysis by including only those terms pertinent to the discussion, cross-coupling, cylindrical, and anisoelastic resonance effects, and coning torques are neglected for the inertially stabilized case. The resulting and basic gyro drift equation is given as

$$D = D_F + D_U + D_K + D_R \tag{1}$$

The D_F drift coefficient is a fixed term dependent on the electromagnetic-element reaction torque and the flex lead torque. Reaction torque is involved in the magnetic suspension of the float and in the microsyn structures of the torque generator and signal generator.

If the acceleration and acceleration squared coefficients are expanded, Eq. (1) becomes

$$D = D_F + D_I a_I + D_O a_O + D_S a_S + D_{II} a_I^2 + D_{SS} a_S^2 + D_{OO} a_O^2 + D_{IO} a_I a_O + D_{IS} a_I a_S + D_{OS} a_O a_S + D_R \tag{2}$$

When the gyro is in the torque-to-balance mode of operation, for instance in a strapdown system, terms resulting from dynamics must also be added to include the angular motion torques (since the gyro is no longer on a stabilized member) and the rebalance loop errors. These terms involve other SLAM gyro parameters that are affected by the design. The linear acceleration torques for the strapdown case are identical to those described for the inertially stabilized case. Since the rebalance loop errors are essentially a function of the torque-to-balance electronics, they are not relevant to this discussion. The angular motion torques remain to be considered. First the torque ($\mathbf{M}_O$) on the float assembly is written in the form

$$\mathbf{M}_O = (d\mathbf{H}_f/dt)_I \tag{3}$$

which describes the rate of change of angular momentum of the float ($\mathbf{H}_f$) relative to inertial space. From this basic equation may be derived the complete equation involving the gyroscopic torque acting along the output axis of an "ideal" single-degree-of-freedom gyroscope ($H\omega_I$) and the other torques resulting from rigid body rotational motion; namely the output axis acceleration torque, anisoinertia torque, gimbal product of inertia torques, cross-coupling torques, and gimbal and rotor misalignment torques.[2] To simplify the discussion, the latter two will not be considered.

Rewriting Eq. (3) relative to the gimbal frame, applying the law of Coriolis, writing the angular momentum of the float assembly as the vector dot product of the float moment of inertia tensor and the angular velocity of the gimbal with respect to inertial space where the float angular momentum is the vector sum of the gimbal angular momentum and the rotor angular momentum, and performing operations with the float and gimbal moment of inertia tensor yields the following equation:

$$M_O = I_{OO}(\ddot{\theta}_O + \dot{\omega}_O) + (I_{II} - I_{SS})\omega_S\omega_I - H\omega_I + I_{OS}(\dot{\omega}_S + \omega_S^2 - \omega_O\omega_I) + I_{OI}(\dot{\omega}_I + \omega_O\omega_S) - I_{SI}\omega_I^2 \tag{4}$$

Gyro drift, Eq. (1), may be rewritten in terms of torques about the output axis as

$$M = M_F + M_U + M_K + M_R \tag{5}$$

and

$$M_i = D_i H : i = F,U,K,R \tag{6}$$

The drift coefficients (D's) are normally expressed in deg/hr or milliearth rate units (0.015°/hr = 1 meru) and the torque coefficients (M's) in dyne-cm. Without conversion factors for Eq. (6), D_i must be in rad/sec and H in dyne-cm-sec for M_i to be in dyne-cm. For a given value of D_i, the lower H is, the lower M_i must be. Thus, a gyro with ten times less angular momentum than a high H unit has ten times more difficulty in achieving a given performance than the high H unit.

Substituting D_i = 1 meru into Eq. (6) yields an expression for the uncertainty torque about the output axis vs wheel angular momentum for a 1-meru performance criterion; $M = 73\ H$ μdyne-cm.

Unless a single-degree-of-freedom instrument, whether it be accelerometer, gyro, or viscous integrator, has a torque stability about its output axis commensurate with its desired performance in a benign environment, there is little point in considering its performance in a dynamic environment. In the case of the gyro, this means that the D_F and D_R coefficients must be considered before one considers the D_I, D_{II}, ... unbalance and compliance terms.

Ideally it is desirable to be completely free of error terms, but in practice this is impossible. Short of this, the approach is to quantify each of the error coefficients and depend upon their magnitude remaining constant such that they may be compensated or accounted for by means of an onboard computer. The magnitude and uncertainty of each of these error coefficients may be related to the design of one or more of the SLAM gyro subassemblies. In terms of those error coefficients involved in the acceleration-insensitive, the linear acceleration, and angular motion error torques; the coefficients of interest are: D_F, D_R, D_I, D_S, D_O, D_{II}, D_{SS}, D_{OO}, D_{IO}, D_{IS}, D_{OS}, I_{OO}, I_{II}, I_{SS}, I_{OS}, I_{OI}, and I_{SI}, all as defined previously. These error coefficients are discussed in terms of which aspect of SLAM gyro technology affects their magnitude and stability, and specifically which gyro technology has been applied to optimize the SLAM gyro performance. Table 1 summarizes each error coefficient and the design technology influencing its magnitude and stability.

Float Suspension

The float of the SLAM gyro is supported in the same manner as most conventional Draper Laboratory single-degree-of-

freedom instruments, by the buoyant force of the flotation fluid, and by a passive magnetic suspension.[3] The suspension rotor is fabricated from ferrite, the permeance of which may not be uniform throughout due to the nonhomogeneity of the ferrite material. As a result, the magnetic suspension produces a torque about the output axis which becomes the major contributor to the reaction torque (T_R) influencing the D_F error coefficient;

$$T_R \propto MMF^2 dP/d\theta \propto (I_{ms}N)^2 dP/d\theta \quad (7)$$

$$T_R = K_1(V/Z_{ms})^2 \quad (8)$$

The variation in reaction torque with suspension excitation voltage is given by

$$dT_R = 2(dV_{ms}/V_{ms})T_R \quad (9)$$

This variation in reaction torque due to suspension excitation voltage variation affects the performance of the SLAM gyro in the following manner. For $T_R = 0.5$ dyne-cm, and $dV_{ms}/V_{ms} = 0.001$ (0.1%), the variation in reaction torque equals $dT_R = 1 \times 10^{-3}$ dyne-cm. For an angular momentum of 8000 dyne-cm-sec, the variation in the acceleration-insensitive drift term corresponding to this variation is $dD_F \approx 2$ meru. Thus, the variation in D_F due to a 0.1% suspension voltage stability would represent a serious performance limitation of the SLAM gyro. For a gyro with an angular momentum of 50,000 dyne-cm-sec, the same value of T_R and variation in suspension excitation voltage would produce a variation in D_F of less than 0.3 meru.

The design of the SLAM gyro circumvents the large dD_F problem by means of a compensation winding that is wound integrally with the suspension windings.[3] The magnetic suspension with the addition of the compensating winding is similar to a two-phase motor winding. When the windings are excited with time-phase displaced currents, a rotating magnetic field is developed. The rotating magnetic field, induced in the ferrite suspension rotor, interacts with the hysteresis ferromagnetic material to create a rotational torque.

The reaction torque magnitude, Eq. (8), and variation with suspension excitation voltage variation, Eq. (9), are compensated so that torque coefficient M_F due to reaction torque and dM_F due to the variation in reaction torque become nearly zero. Hence, drift coefficients D_F and dD_F correspondingly become nearly zero.

Currently under development to replace the passive magnetic suspension is an active magnetic suspension. The passive suspension requires a constant input power, and has a nearly linear displacement vs force characteristic. In general, more stiffness means more power and/or a larger volume. Active suspension is a major advance in float suspension technology in that it requires very low power when low force inputs are applied to the float, and it has a lower power requirement than passive suspension for the same force input. The force vs displacement curve for active suspension can be a high-order function of displacement, and, in general, can be tailored within certain broad limits to achieve a much higher stiffness. Active suspension can be utilized to minimize the float displacement radially and axially when the gyro is subjected to extreme environments.

Table 1 Design aspects influencing error coefficients

Error coefficient	Design aspect
D_F	Output-axis float magnetic suspension, signal generator, and torque generator design; flex lead torques
D_I, D_S	Float balance capability along spin and input axes
D_{IS}, D_{OS}	Angular momentum generator (spin motor) design
I's, D_{II}, D_{SS}, D_O, D_{IO}	Float design
D_R	Thermal and total assembly stability, fluid homogeneity, basic material stability
D_{OO}	Negligible magnitude

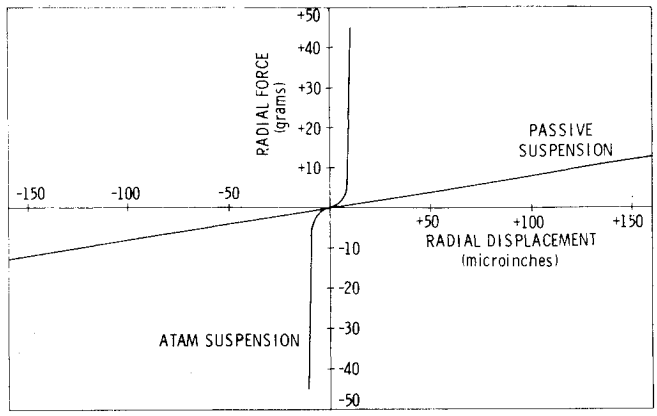

Fig. 2 Radial stiffness, passive vs active suspension.

The lower the float displacement and the lower the suspension power for a given force input to the float means that, in general, the lower will be the uncertainty torques about the output axis. Ideally, it would be desirable to have no suspension force with no force input to the float and, thus, no uncertainty torques due to the suspension. This is particularly ture to space applications where force inputs to the float near zero are achievable.

The active suspension utilizes the same suspension stator coil and rotor configuration as the passive suspension, except that the volume may be made smaller by decreasing the number of stator turns and the volume of stator iron and rotor ferrite. Such a change in the SLAM gyro could halve the float output-axis inertia.

Figure 2 shows a plot of the stiffness of the active suspension vs the passive suspension.

Signal Generator and Torque Generator

The signal generator (SG) of the SLAM gyro is a variable reluctance angle-to-voltage transducer known as a microsyn. The rotor is a ferrite material secured to the float and the stator is an assembly of bonded laminations containing twelve poles with wirewound coils interconnected to provide an E-type configuration.

Normally, the performance of the single-degree-of-freedom gyro is affected by the elastic restraint (K_{ER}) of the microsyn; however, the design of the SLAM gyro eliminates elastic restraint by compensation. This is achieved by subtracting and adding the necessary amount of energy from the appropriate poles as the rotor is displaced angularly. A capacitor is added across the secondary winding to load the winding and draw a given current (in-phase with the primary current) that is proportional to angular displacement.

The SLAM gyro employs a dual permanent-magnet torque generator, one on each end of the float. The permanent-magnet structure consists of an N-pole composite magnet with a soft-iron return path and a torquing coil assembly. The magnet is composite in that the magnet ring and poles are made of different materials. A high permeability material such as Carpenter 49 is used for the ring and Alnico IX poles

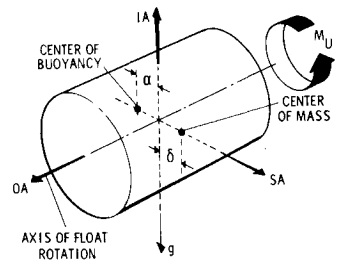

Fig. 3 Float balancing analysis.

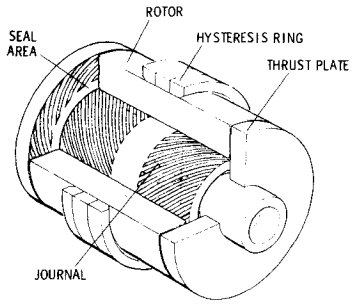

Fig. 4 Angular momentum generator.

are mounted to it. The advantage of the soft-iron ring is that due to its high permeability relative to a normally used hard iron (25×10^3 larger), fringing between the permanent magnet and the suspension inside of the ring is eliminated. The coils are mounted on a holder attached to the float, and they are excited through flex leads.

Viscous Integrator

The preceding paragraph discussed the torques about the gyro output axis that contribute to the drift coefficient D_F. The evaluation of the uncertainty of these torques and the contributors to D_R, such as flotation fluid thermal torques, and random components of the electromagnetic element torques can best be accomplished by means of a viscous integrator. This interim test vehicle consists of a solid float with ferrite rotors on each end supported by flotation fluid and magnetic suspension. A microsyn signal generator is at one end and a torque generator at the other end. Thermal control of the instrument is identical to that of the final instrument; integrally wound heater-sensor windings are on the ends and belly of the case as part of a proportional-type temperature control system. Flotation fluid and electromagnetic element gaps are identical to the final gyro design. The float is balanced about the output axis by using the techniques described later.

The performance of the viscous integrator (operated in the torque-to-balance mode by means of an analog servo) evaluates the magnitude and uncertainty of all compensated torques previously described and all of the contributors to the D_F term, except flex-lead torque and those torques produced by the internal float thermal conditions generated by wheel power. (However, a viscous integrator with flex leads has been tested.) Test results to date indicate a long-term (days) OA torque stability of 200 μdyne-cm peak-to-peak (the equivalent of 0.3 meru) for a unit with an angular momentum of 8000 dyne-cm-sec. Short term (hr) torque stability is 80 μdyne-cm peak-to-peak with both the microsyn and suspension reaction torque and the microsyn elastic restraint compensated.

Float

The float consists of the main gimbal structure, the angular momentum generator and its supports, flotation weights, two magnetic suspension and microsyn rotors, and flex lead terminals. The design of this structure is critical to the performance of the SLAM gyro since it is the torque summing member. Design of the float encompasses many facets of engineering technology such as material behavior, magnetism, strength of materials, chemistry, heat transfer, and thermodynamics. Some of the considerations in the design of the float are that it be as symmetrical as practically possible about the output and spin axes and that the float inertias, differences of inertias, and product of inertias be as small as possible. Choice of float materials is extremely important from the standpoint of dimensional and thermal stability, ease of machining, surface finishes obtainable, and compatibility with the materials such as adhesives, potting compounds, and flotation fluid. This last item is particularly important in light of the degree of activity of some of the high-density gyro flotation fluids. Float material properties which are particularly desirable are low porosity, nonmagnetic, high strength-to-weight ratio, and high thermal conductivity (to minimize float hot spots). Other considerations in float design are the use of materials with matched thermal coefficients of expansion and the assurance that all parts of the final assembly be as stress-free as possible to minimize creep.

The error coefficients relative to the float are the unbalance terms, the inertia terms, most of the compliance terms, and D_O. The first terms to be considered are unbalance terms D_I and D_S, which result from float unbalance about the output axis along the spin and input axes, respectively[4];

$$D_I = U_S g_I/H, D_S = U_I g_S/H \tag{10}$$

Using the terminology and considering the orientation of the unit with respect to g defined in Fig. 3, the unbalance torque about the output axis in a one-gravity field is

$$M_{US} = -g(\alpha M + \delta M) \tag{11}$$

This equation is true only if the flotation fluid density is such as to put the float at neutral buoyancy. If the float is not at neutral buoyancy, Eq. (11) becomes

$$M_{US} = -\alpha[Mg + (d_{\rho f}/dT)V\Delta T] - \delta Mg \tag{12}$$

From Eq. (12), it can be seen that the unbalance sensitivity to temperature is:

$$\Delta M_{US}/\Delta T = -\alpha(d_{\rho f}/dT)V \tag{13}$$

The quantities $d\rho_f/dT$ and V are known, and for a given gyro temperature change, terms ΔT and ΔM may be measured. Thus term α may be computed. Further, by knowing M_{US} at its flotation temperature, term δ may be computed from Eq. (11).

The task of float balancing involves making both α and δ as small as possible to minimize the float unblance magnitudes and temperature sensitivity. The means by which this is accomplished in a gyro of larger size is through the use of adjustable balance weights on the float. In the SLAM gyro, this becomes impractical because of the small float size and the instability of typical unbalance correction hardware when the unit is subjected to extreme environments. For example, a 10-μin. shift in a 30-mg balance weight produces a gyro unbalance coefficient (D_I,D_S) shift of 1 meru/g (H = 8000 dyne-cm-sec). The approach to balancing is to first perform a coarse balance in a tank by means of a limited number of weights which are then permanently fixed. Following this, the unit is final-assembled and then tumble-tested to determine precisely the gyro unbalance coefficients and values of α and δ. The gyro is then fine balanced (making α and δ as nearly zero as possible) by removing a controlled amount of material from the float.

By using electrical discharge machining (EDM), the material removal can be achieved without disassembly of the gyro. The gyro is placed in a fixture with EDM probes that go through small holes in the case. Fine balancing is achieved with the gyro in the flotation fluid and operated in the torque-to-balance mode while being tumbled about the output axis. A vacuum system on the probes removes the machined material from the gyro. The advantage of this method is that the gyro does not have to be disassembled, which can cause changes in float balance. Flex lead changes can change the unbalance by as much as 1 meru/g (H = 8000 dyne-cm-sec). Initial experiments with EDM indicate that a resolution of less than 0.5 meru/g is feasible.

The last unbalance term is D_O, which is due to an apparent unblance along the output axis;

$$D_O = U_O g_O/H \tag{14}$$

Unlike the other mass unblance terms whose physical significance can be easily grasped, the physical source of this term that is proportional to acceleration along the output axis is

difficult to identify. The cause of this term was identified on a larger inertial gyro to be primarily due to thermal convection forces of the fluid around the float balance hardware. Since the SLAM gyro has no float balance hardware, and since the float is completely free of any holes or indentations around its periphery, it presents no known mechanisms for the D_O term.

The remaining compliance terms to be discussed are D_{IO}, D_{II}, D_{SS}, and D_{OO}. There is no known gas-bearing wheel mechanism for any of these terms. The compliance coefficients relative to the float may be expressed as

$$D_{IO} = K_{SO}m^2/H,\ D_{II} = K_{SI}m^2/H \tag{15}$$

$$D_{SS} = -K_{IS}m^2/H,\ D_{OO} = K_{OO}m^2/H \tag{16}$$

There is no known mechanism for displacement of a gas bearing along its spin axis due to an acceleration along the input or output axis. Test results from larger gyros, when compared to similar tests on viscous integrators, indicate that two possible mechanisms exist for these terms. The first is the true float compliance, and the second is due to the variation in wheel power with acceleration. An acceleration force on the gyro affects its operation by changing the gas-bearing load on the motor, which in turn changes the motor torque applied to maintain wheel synchronism. A change in power flowing to the motor can furthermore have a secondary influence on gyro torque because of the difference in thermal dissipation. This thermal change may affect the gyro unbalance due to thermal deformation and cause fluid flow torques. No measurements have been made in the SLAM gyro to ascertain to what degree such an effect is present and whether it varies as g^2 so as to appear as a compliance term.

The error coefficients I_{OO}, $I_{II} - I_{SS}$, I_{SO}, I_{OI}, and I_{SI} are associated with the float design. The difference of inertia term ($I_{II} - I_{SS}$) and the product of inertia terms (I_{OO}, I_{OS}, and I_{OI}) can be made very small. The computed value of the product of inertia term indicates that they are less than 0.005 g-cm.^{2} From Eq. (4), the error torque due to these terms for the strapdown system case is the product of the product of inertia with either a body angular rate squared or the product of two orthogonal body rates. When the product of inertia term is 0.005 g-cm^2 and the body rates are 0.5 rad/sec, the resulting gyro output is equivalent to 2 meru for an $H = 8000$ dyne-cm-sec.

For the application of the SLAM gyro (or any gyro) to a strapdown system, the gyro outputs resulting from the product of body angular rates with the difference of inertia term should be compensated with a computer (depending upon the system accuracy required). The same is true for the product of the OA inertia and angular acceleration about the output axis. The computer compensation of both these terms is part of the strapdown mechanization. For the SLAM gyro, a difference of inertia of 0.1 g-cm^2 coupled with body rates about the input and spin axes of 0.5 rad/sec results in a gyro output the equivalent of 40 meru ($H = 8000$ dyne-cm-sec). On the other hand, the OA inertia of the SLAM gyro coupled with a tyipcal space vehicle body angular acceleration results in a gyro output the equivalent of greater than hundreds of meru.

Angular Momentum Generator

Error coefficients related to the angular momentum generator are the compliance torques due to the anisoelastic structure of the float (D_K) as given by Eq. (2). Two of the terms in Eq. (2) are affected by the design of the angular momentum generator: namely, terms D_{IS} and D_{OS}. This is particularly true for hydrodynamic gas-bearing wheels such as the spool gas-bearing design in the SLAM gyro. Before describing the spool design and its design features that enhance the performance of the SLAM gyro, a brief description of the mechanisms for the terms is in order.

The D_{IS} and D_{OS} terms result from the fact that, for a radial load such as acceleration on the rotating mass of the wheel, a gas bearing need not deflect in the same direction as the load. The angle between the load and the deflection is called the attitude angle. Thus, loading along the output axis can give rise to a deflection along the input axis of

$$d_I = K_R a_O M_W \sin A_a \tag{17}$$

If a force exists along the spin axis, this gives a drift rate of

$$W_d = d_I a_S M_W/H = K_R a_S a_O M^2 \sin A_a/H \tag{18}$$

or

$$D_{OS} = K_R M_W^2 \sin A_a/H \text{ (minor compliance term)} \tag{19}$$

In a similar manner, the major compliance term is

$$D_{IS} = (K_A - K_R \cos A_a)M^2/H \tag{20}$$

Note that K_A and K_R are not to be confused with K_{II} and K_{SS}, which are the reciprocal of K_A and K_R, respectively.

Using the wheel parameters of $K_R = 50$ μin./mg, $M_W = 5$ g, $H = 8000$ dyne-cm-sec, assuming a maximum allowable value of $D_{OS} = 1$ meru/g^2, and solving Eq. (19) for A_a yields the maximum allowable value of $A_a = 11°$. This attitude angle and less has been achieved in the wheel design. Considering the major compliance term, with an 11° attitude angle, K_A may be mismatched from K_R by 18% to yield a D_{IS} term of less than 1 meru/g^2. Again less than this degree of mismatch has been achieved through careful design of the radial and axial bearings of the SLAM gyro wheel.

The gas-bearing gyro wheel for the SLAM gyro is an end-thrust type, spool, hydrodynamic gas bearing. The basic principle of operation of this wheel is that the rotor rides on a thin film of pressurized gas, between the rotor and stationary journal and thrust plates. The rotor is gas-borne, with low friction, the only rubbing occurring during starting and stopping.

The gyro wheel consists of a journal, two thrust plates, a rotor, and a hysteresis ring (Fig. 4). The journal is a solid shaft which contains herringbone pumping grooves to eliminate rotor half-frequency whirl and to generate supra-ambient internal rotor support pressures. The thrust plates have whipple grooves extending to the outside diameter for maximum pressure flow, and with a dam on the inside diameter to minimize gas leakage. The rotor is a simple annular cylinder which operates free of contact from the thrust plates and journal. The hysteresis ring is a laminated ring which has hysteresis properties to provide wheel driving torque. The journal, rotor, and thrust plates are fabricated from fine-grain boron carbide, which appears to be virtually wear-free. The main feature of the boron carbide wheel is the manner in which the material enhances the wheel performance. The grade of boron carbide used was designed particularly for the SLAM gyro application. The characteristics of the boron carbide material are discussed later.

The rationale behind the wheel design is that there are inherent benefits resulting from gas-bearing miniaturization. Because of the low angular momentum, a high slew capability is achieved. The low rotor weight combined with a high surface area of support per unit of volume, compared to a high angular momentum wheel, means a high acceleration and slew capability. The small size of the wheel also enhances its thermal and mechanical stability, resulting in low thermal expansion and creep characteristics. Even with more than adequate torque reserve from the hysteresis motor, which results in no hunting, the input power is low due to the low drag torque. The wheel does not require overvoltage to start and has a rapid run-up and run-down time with the rotor not rotating at the stopping point during run-down due to pre-touchdown oscillation. Therefore, wear during the stop-cycle of the rotor is practically nonexistent. As a result, no lubricant is used on the gyro wheel. High-performance gas bearings require microinch geometric tolerance of the critical surfaces that determine the degree of gas pressurization avail-

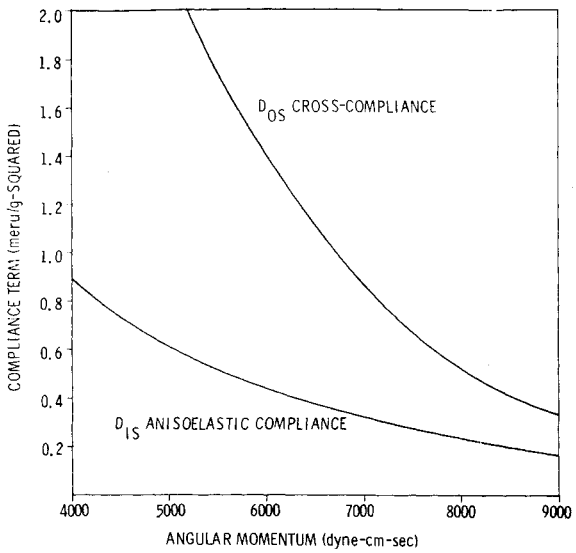

Fig. 5 Gas bearing compliance terms vs angular momentum (wheel speed variation).

able for support of the rotating mass. The wheel design used has been exclusively the spool-type configuration for ease of fabrication; that is, the plane and cylindrical surface are easily manufactured and inspected. The machining tolerances are on the order of 5 μin., which is now achievable in production. In conjunction with the design, manufacture, and testing of miniature-type gas bearings, a theoretical analysis has been used by means of a computer program to facilitate predicting the performance and to optimize the design of the spool-type gas bearing. The slew capability of the wheel vs wheel angular momentum (wheel speed variation) over a range of 4000–9000 dyne-cm-sec increases linearly from 110 to 120 rad/sec. The radial g capability increases linearly from 275 to 650 g and the axial varies linearly from 400 to 900 g over the same angular momentum range.

Figure 5 shows compliance terms as a function of wheel angular momentum. The nominal running torque is given by the following equation, except for values of H <4000 dyne-cm-sec:

$$R = 371H - 184 \qquad (21)$$

The boron carbide wheel technology replaces a wheel manufactured in high quantity which has beryllium shaft and thrust plates and a rotor of a glass-ceramic material, pyroceram. Although that wheel has operated in thousands of units for millions of hours with a low failure rate, the design has definite deficiencies. Specifically, the main deficiencies are that pyroceram does not have sufficient wear resistance and tends to deposit itself in the thrust plate grooves when high speed touchdown occurs; this results in a decreased gap and subsequent possible failure of the rotor to start. The other deficiency is that it is difficult to control contamination on the machined surfaces because of the porosity of beryllium. Also, the beryllium thrust plates and shaft require the application of a boundary lubricant for stop-start reliability.

Boron carbide (B_4C) is a hard, stiff ceramic with a specific gravity of 2.52, readily lending itself to gas-bearing and other precision-instrument applications. Commercially formed by biaxial hot-pressing of fine B_4C powder (formed by a number of chemical processes) at temperatures typically in the 2000°C range, the resulting material has greater than 99% of theoretical density (2.52 g/cm^3 or 156 lb/ft^3). It is also possible to achieve a total of boron and carbon content of greater than 99% (that is, total impurities less than 1%), although some of the carbon may be uncombined with boron. This free carbon can be of the order of $\frac{1}{2}$% to 1%, and never more than 2%. Typical of this polycrystalline material is a hardness of 2800–3000 on the $Knoop_{100}$ scale (second only to diamond at ≈7000, and the newly developed and introduced cubic boron nitride at ≈4400). Hardened bearing steels are typically in the $Knoop_{100}$ 700 range. Also, the Young's (or elastic) modulus for boron carbide (65 million) is greater than that for beryllium (44 million), lending to the usefulness of boron carbide in both bearing and structural loads. Figure 6 shows a plot of the modulus of elasticity vs specific gravity for various materials.

One supplier currently has a high-density, high-purity boron carbide with a 5-μ average grain-size, while most commercial samples typically show an average grain-size of 20 to 30 μ or more. Two development programs have been instituted with the intent of producing a superior quality polycrystalline boron carbide. One program goal is the achievement of an average grain-size of less than 1 μ (40 millionths of an inch). It is, of course, desirable to improve other properties as well as grain-size (porosity, purity, hardness, etc.), but they are often related to a fine-grained material, and grain-size often indicates these other parameters.

Boron carbide wheels do not require a boundary lubricant as the beryllium-pyroceram wheel did. Initial wear-testing of unlubricated boron carbide against boron carbide led to a somewhat perplexing discovery—that the surface finish of the boron carbide improved considerably as wear-testing continued. Further investigation and development of this phenomenon led to what is now called the boron-carbide, high-speed dry-lapping technique. This lapping technique has advanced to the point where surface finishes attainable on boron carbide are equalled by those of only a few other materials.

The characteristics of the boron-carbide dry-lapped surface are the following. 1) Surface finish: the surface finish of a sample after dry lapping is less than 1 μin. AA, and estimated to be 0.1 μin. AA and scratch-free. 2) High reflectivity: dry-lapping produces a mirror-like surface on the sample. This is very helpful in showing up dust particles, fingerprints, and other forms of contamination that would be detrimental to the operation of the gas bearing. 3) Coefficient of friction: preliminary tests indicate that the coefficient of friction of two boron carbide samples sliding against one another is approximately 0.09 (uniform slip on an inclined plane). 4) Geometry: critical surface conditions (roundness and flatness) are easy to produce with the dry-lapping technique. Extensive testing in this area has shown that small parts can be rough lapped to a flatness of 10 μin. and final lapped to a flatness of less than 5 μin. with no difficulty. 5) Decreasing wear-rate: the wear produced by the dry-lapping technique is probably the most interesting feature possessed by boron-carbide. Test data indicate that for a constant force applied to a sample with a constant surface speed, the wear per unit

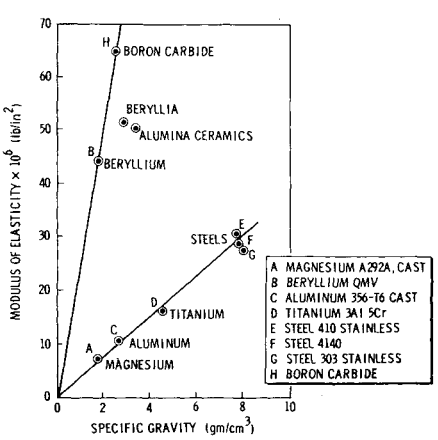

Fig. 6 Modulus of elasticity vs specific gravity for various gas bearing materials.

to time decreases during the lapping operation. This feature if of particular importance in gas-bearing performance; typical operating clearances in a high-performance gas bearing are 40 μin., and these clearances are considerably reduced under load. If at any time the bearing were to be overloaded and moving parts touched, wear particles could be generated and cause catastrophic failure of the gas bearing. A bearing made of boron carbide with dry-lapped running surfaces, however, reduces this possibility considerably.

Conclusions

The feasibility of the SLAM gyro is very dependent upon the magnitude and stability of drift coefficients D_F, D_U, D_K, and D_R of Eq. (1). Due to the relationship stated in Eq. (6), to achieve this requisite with a low angular momentum means that each term's contributions to uncertainty torque about the output axis must be small compared to the signal torque. This must be true in a benign as well as an extremely dynamic environment (external accelerations and angular accelerations). To quantify small, an input rate of 1 meru to a gyro with an angular momentum of 8000 dyne-cm-sec results in a torque about the output axis of about 600 μdyne-cm. The achievement of a torque uncertainty about the output axis due to D_F, D_U, D_K, and D_R of this value is the technology of the SLAM gyro.

The SLAM gyro is well suited for strapdown guidance system applications for the following reasons: a) the ability of the angular momentum generator to withstand high angular rates; b) a low angular momentum, which means the *TG* generated torque to balance the torque due to the input rates is low when compared to a unit with a high angular momentum; c) because of item b and the use of a dual permanent-magnet torque generator, the power required by the torque generator for high rates is extremely low (less than $\frac{1}{4}$ w for 60°/sec); d) the permanent-magnet torque generator design has the linearity, hysteresis, and scale factor stability commensurate with the requirements of high accuracy strapdown systems.

References

[1] Palmer, P. J., "Gyro Torque Coefficients," E-1601, Dec. 1964, Charles Stark Draper Lab., MIT, Cambridge, Mass.

[2] Gelb, A. and Sutherland, A., Jr., "Design of Strapdown Gyroscopes for a Dynamic Environment," Semi-Annual Rept., July 1967, Analytic Sciences Corp., Winchester, Mass.

[3] Frazier, R. H., Gilinson, P. J., Jr., and Oberbeck, G. A., *Magnetic and Electric Suspensions, as Developed in the Charles Stark Draper Laboratory*, to be published, MIT Press, Cambridge, Mass., and London, England.

[4] Hazel, M. E., Jr., "Evaluation of Inertial Gyroscope Static Float Balance Techniques," R-530, Dec. 1965, Charles Stark Draper Lab., MIT, Cambridge, Mass.

SEPTEMBER 1971 J. SPACECRAFT VOL. 8, NO. 9

Frequency Stability Characteristics and Stabilization Techniques in an SSB-FDMA/PhM Multiple Access System

S. J. ANDRZEJEWSKI*
Westinghouse Electric Corporation, Defense and Space Center, Baltimore, Md.

The system is described and its frequency stability characteristics and stabilization techniques are investigated and analyzed. Utilizing Fourier analysis techniques, the causes of the test tone frequency instability are identified and measured. The system's present AFC unit is described in detail and its shortcomings from the standpoint of reducing the instability factors are presented. Alternate AFC configurations are discussed and the most promising technique (called the reference carrier technique) found to date is described in detail. This entails a description of the instrumentation of the technique and its advantages and disadvantages from a system standpoint. Also the equations that determine the degree of stability compensation are derived and the requirements for optimum compensation are determined. Measurements are presented to show the degree of compensation obtained and the various factors that affect it. It was found that the technique has an amplification effect on thermal noise thus causing an increase in the noise components at frequencies greater than the test tone frequency. Because of the aforementioned effect and the fact that the baseband noise spectrum varies linearly with frequency, the limiting condition for the reduction of the instability is thermal noise.

Introduction

ONE of the communication experiments that is being conducted on a series of Applications Technology Satellites (ATS) utilizing three ground stations (Mojave, California; Rosman, North Carolina and Cooby Creek, Australia) is the testing of a unique SSB-FDMA/PhM multiple access system.

The experiment is being conducted on two spin stabilized geostationary satellites (ATS-1 and ATS-3) as a part of the NASA/Goddard Space Flight Center Applications Technology Satellite Program. During the test phase, it was noted that an excessive amount of short-term frequency variations were present on the test tone at the output of a receive multiplex channel. These variations are due in part to incidental angle modulation impressed on the test tone

Presented as Paper 70-411 at the AIAA 3rd Communications Satellite Systems Conference, Los Angeles, Calif., June 6, 1970; submitted August 17, 1970. Many of the concepts and test data presented in this paper were obtained from individuals at ATS headquarters located in GSFC and personnel from the three ground stations; Mojave, California, Cooby Creek, Australia and Rosman, North Carolina. In particular I would like to thank E. Metzger, Operations Chief and R. Darcey, Chief of the ATS program for their cooperation and aid in obtaining the required test data.

* Senior Engineer, Field Engineering and Support.